GFZ
Helmholtz-Zentrum
POTSDAM

Intercomparisons of Rainfall Estimates from TRMM and GPM Multisatellite Products over the Upper Mekong River Basin

ZHIHUA HE[a]

Department of Hydraulic Engineering, Tsinghua University, Beijing, China

LONG YANG

Department of Civil and Environmental Engineering, Princeton University, Princeton, New Jersey

FUQIANG TIAN AND GUANGHENG NI

Department of Hydraulic Engineering, Tsinghua University, Beijing, China

AIZHONG HOU

Hydrology Bureau, Ministry of Water Resources, Beijing, China

HUI LU

Ministry of Education Key Laboratory for Earth System Modeling, and Department of Earth System Science, Tsinghua University, and Joint Center for Global Change Studies, Beijing, China

ABSTRACT

The aim of this study is to evaluate the accuracy of daily rainfall estimates based on the GPM level-3 final product derived from the IMERG algorithm (abbreviated as IMERG) and TRMM 3B42, version 7 (abbreviated as 3B42), in the upper Mekong River basin, a mountainous region in southwestern China. High-density rain gauges provide exceptional resources for ground validation of satellite rainfall estimates over this region. The performance of the two satellite rainfall products is evaluated during two rainy seasons (May–October) over the period 2014–15, as well as their applications in hydrological simulations. Results indicate that 1) IMERG systematically reduces the bias value in rainfall estimates at the gridbox scale and presents a greater ability to capture rainfall variability at the local domain scale compared with 3B42; 2) IMERG improves the ability to capture rain events with moderate intensities and presents higher capability in detecting occurrences of extreme rain events, but significantly overestimates the amounts of these extreme events; and 3) IMERG generally produces comparable daily streamflow simulations to 3B42 and tends to outperform 3B42 in driving hydrological simulations when calibrating model parameters using each rainfall input. This study provides an early evaluation of the IMERG rainfall product over a mountainous region. The findings indicate the potential of the IMERG product in overestimating extreme rain events, which could serve as the basis for further improvement of IMERG rainfall retrieval algorithms. The hydrological evaluations described here could shed light on the emerging application of retrospectively generated IMERG products back to the TRMM era.

1. Introduction

Precipitation is a key variable representing mass exchange and energy balance in the climate system and thus plays a significant role in hydrometeorology-related applications (Brutsaert 2005; Wanders et al. 2015). The timing and magnitude of precipitation are of great importance for freshwater supplies and for forecasting of extreme events such as floods and droughts. For hydrological modeling at the basin scale, it is essential to obtain high-quality estimates of precipitation in both space and time (Livneh et al. 2014). This issue is more prominent in mountainous basins, where precipitation presents large spatial variability due to strong

[a] Current affiliation: Section 5.4 Hydrology, GFZ German Research Centre for Geosciences, Potsdam, Germany.

Corresponding author e-mail: Fuqiang Tian, tianfq@mail.tsinghua.edu.cn

topographic transitions and is typically poorly covered with gauges (Wang and Lin 2015). Satellite rainfall estimates prove to be promising in providing reasonable representations of space–time features of rainfall in these regions (Xu et al. 2015).

A number of quasi-global satellite rainfall products have been developed since the 1980s, such as Precipitation Estimation from Remotely Sensed Information Using Artificial Neural Networks (PERSIANN; Sorooshian et al. 2000), the National Oceanic and Atmospheric Administration/Climate Prediction Center (NOAA/CPC) morphing technique (CMORPH; Joyce et al. 2004), the Tropical Rainfall Measuring Mission (TRMM; Huffman et al. 2007), Global Satellite Mapping of Precipitation (GSMaP; Ushio et al. 2009), and the Naval Research Laboratory (NRL)-developed blended-satellite rainfall technique (NRL-Blend; Turk et al. 2010). Extensive studies have evaluated these satellite rainfall products in a variety of climate settings (Dinku et al. 2007; Shen et al. 2010; Jiang et al. 2012; Krakauer et al. 2013). The latest version of the gauge-adjusted TRMM product 3B42, version 7 (3B42V7), with a spatial resolution of $0.25° \times 0.25°$, has often exhibited high performance (Sapiano and Arkin 2009; Liu et al. 2015; Salio et al. 2015). For instance, Tong et al. (2014) found that the TRMM 3B42V7 rainfall product performs better in both of monthly and daily streamflow simulations than CMORPH, PERSIANN, and 3B42 real time (3B42RT) products over the Tibetan Plateau. Xue et al. (2013) also demonstrated that TRMM 3B42V7 generally outperforms TRMM 3B42, version 6 (3B42V6), with higher skill scores in the Wangchu basin in Bhutan.

Despite these widespread applications, the underperformance of the TRMM 3B42V7 product is still obvious, especially in mountainous areas (Meng et al. 2014). For instance, Zhao et al. (2013) found that the 3B42V7 product is insufficient in reflecting the strong impacts of topography on rainfall over mountainous basins in northwestern China. The coarse spatial resolution poorly captures rainfall variability over regions with strong topographic transitions and thus may misrepresent extreme rain events (Castro et al. 2015).

As the successor of TRMM, the Global Precipitation Measurement (GPM) mission, led by the National Aeronautics and Space Administration (NASA) and the Japan Aerospace Exploration Agency (JAXA), has begun to provide the next generation of rainfall products (Hou et al. 2008). The GPM mission consisted of one *Core Observatory* satellite and nine constellation satellites over the study period. The GPM *Core Observatory* was successfully launched on 28 February 2014. This *Core Observatory*

carries a dual-frequency precipitation radar (DPR; the Ku band at 13.6 GHz and Ka band at 35.5 GHz) and a multichannel GPM Microwave Imager (GMI), which will be used together to develop a new calibration standard for other microwave radiometers on the constellation satellites (Tapiador et al. 2012; Yong et al. 2015). In particular, the *Core Observatory* will extend the measurement range attained by TRMM to include light-intensity precipitation (<0.5 mm h^{-1}; Hou et al. 2014).

One of the GPM products is based on the Integrated Multisatellite Retrievals for GPM (IMERG), which is the unified U.S. algorithm and provides a multi-satellite rainfall product (Kidd and Huffman 2011; NASA 2015). The algorithm system is run twice in near–real time, that is, the ''Early'' multisatellite product approximately 6 h after observation time and the ''Late'' multisatellite product approximately 18 h after observation time, and once after the monthly gauge analysis is received, that is, ''Final'' satellite–gauge product approximately 3 months after the observation time (Huffman and Bolvin 2015). The Early run only performs forward propagation of the microwave data, whereas the Late run and Final run have both forward and backward propagations of the microwave data. All of the three runs generate half-hourly products at a spatial resolution of $0.1° \times 0.1°$, and the final post-real-time run additionally creates a monthly dataset. The near-real-time early and late half-hourly estimates are calibrated with climatological coefficients, whereas the final post-real-time, half-hourly estimates are adjusted based on satellite–gauge combined monthly data.

It is expected that the first retrospectively reprocessed IMERG products using TRMM will be released in early 2017, which will provide a long IMERG record for hydrological application. Thus, it is necessary and meaningful to conduct ground validation of IMERG data and to investigate how the retrieval algorithm performs based on recently released products. Worldwide, projects focusing on ground validation of GPM products are underway, for example, the Integrated Precipitation and Hydrology Experiment (IPHEx; Barros et al. 2014). Early comparisons have preliminarily revealed the performance differences between TRMM-era products and IMERG. For instance, the IMERG monthly product can capture major heavy-rainfall regions in the Northern and Southern Hemispheres reasonably well, and differences between IMERG and 3B42V7 vary with surface type (land or ocean) and rainfall rate (Liu 2016). At the regional scale, the Day-1 IMERG considerably outperforms 3B42V7 at both subdaily and daily time scales in mainland China
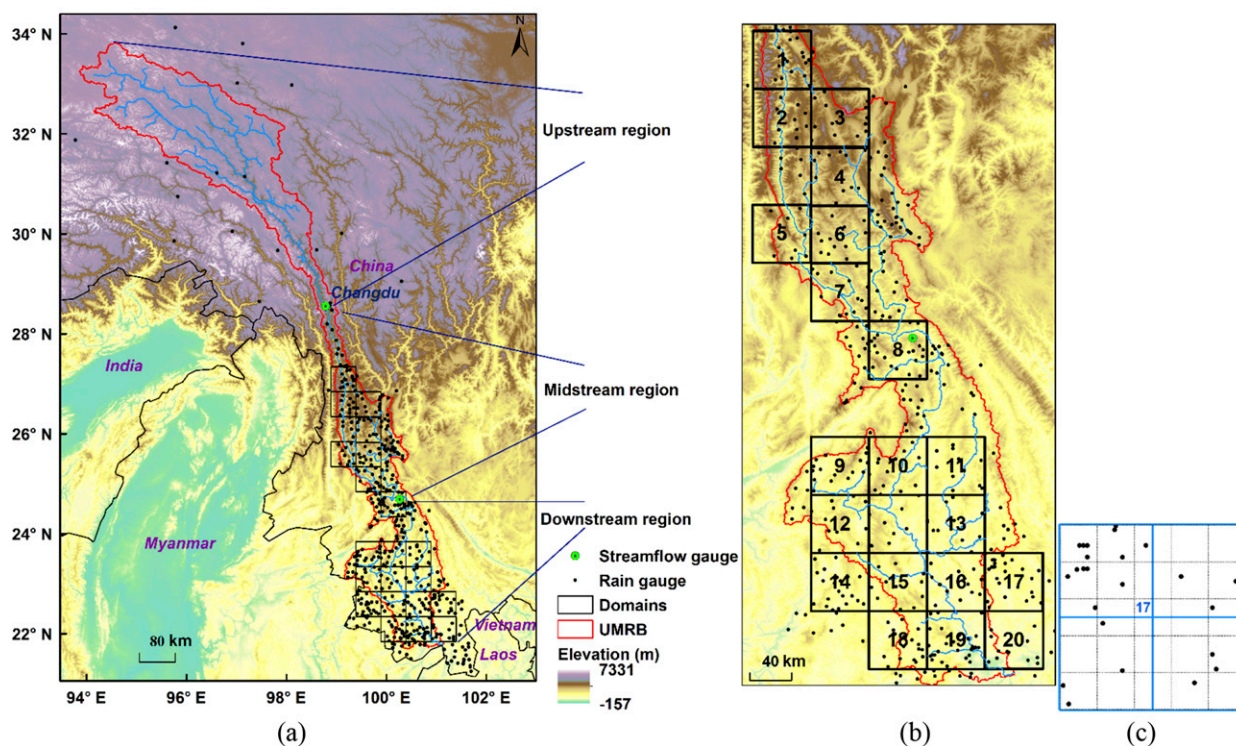
FIG. 1. Study area and locations of the 503 rain gauges.

([Tang et al. 2016a](#)). [Prakash et al. (2016)](#) showed that the IMERG product is superior in capturing heavy rainfall over India. However, limited studies have focused on the performance of the IMERG product over mountainous basins.

In this study, we expect to provide useful insights into the performance of the IMERG retrieval algorithm over mountainous regions and examine how the newly released GPM product differs from its predecessor TRMM 3B42V7. Specific questions that will be examined include the following:

1) Does the IMERG product produce a lower systematic bias value than the 3B42V7 product over mountainous basins?
2) How does the performance of the IMERG product depend on rainfall intensity?
3) What is the potential of the IMERG product in hydrological application over mountainous basins?

Our study region is the upper Mekong River basin (UMRB), which is on the southwestern border of mainland China. A high-density network of rain gauges provides an exceptional resource for the ground validation of satellite rainfall products. To the best of our knowledge, this study is among the first to evaluate GPM rainfall products over mountainous regions, and we expect to shed light on the subsequent improvement

of GPM rainfall retrieval algorithms over regions with similar topographic characteristics.

The paper is organized as follows. In section 2, we describe the study region and introduce rainfall data used in this study. Methods for the intercomparisons of the IMERG and 3B42V7 products, as well as a brief description of the hydrological model, are provided in section 3. Section 4 presents the evaluation results obtained for different rainfall products. Finally, section 5 provides a summary of our findings and concluding remarks.

2. Study area and data

The UMRB (also known as Lancang River in China) is located in southwestern China. It comprises 24% of the Mekong River basin and provides 15% of the total annual flow volume ([Manh et al. 2015](#); [He et al. 2017](#)). The UMRB serves as the most important freshwater source for the downstream riparian countries (including Myanmar, Laos, Cambodia, Thailand, and Vietnam). The upper Mekong River flows from north to south and drains an area of approximately $1.5 \times 10^5 \, \text{km}^2$ ([Fig. 1a](#)). The UMRB is characterized by strong geomorphologic gradients, with an elevation ranging from 516 to 6457 m MSL. The average elevation is approximately 3325 m MSL ([Shi et al. 2013](#)). The

upstream region of UMRB has an average elevation of 4500 m MSL, covered by 18 rain gauges (Fig. 1a). The midstream region shows the sharpest topographic transition and has an average elevation of 2980 m MSL, with 162 rain gauges located in this region. The downstream region contains 323 rain gauges and has an average elevation of 1580 m MSL. Precipitation concentrates in the rainy season from May to October because of the prevalence of the East Asian monsoon.

The entire UMRB features 503 rain gauges (see Fig. 1a for spatial distribution), which are not included in the GPCC gauge network used in both of IMERG and 3B42 ground calibrations. The rain gauge network is deployed and maintained by the Hydrology Bureau, Ministry of Water Resources, China, and has provided observations of daily rainfall since 2014. A day is defined as from 0800 to 0800 of the following day in local time (i.e., 0000–0000 UTC of the following day). Strict quality control procedures have been implemented, ensuring no missing or erroneous records. In the downstream and midstream regions, the densities of rain gauges are approximately 10 per 1000 km^2 and 4 per 1000 km^2, respectively. The density of rain gauges then decreases to 0.24 per 1000 km^2 in the upstream region. Our densities of rain gauges are exceptionally higher than those in previous studies conducted in the UMRB [e.g., less than 70 gauges over the entire basin, and less than 10 gauges in the upstream region used by Zhang et al. (2011), and Zeng et al. (2013)].

Both the TRMM 3B42V7 product (3-hourly; abbreviated as 3B42 hereinafter) and the GPM level-3 final product based on the IMERG algorithm (half-hourly; abbreviated as IMERG hereinafter) were integrated into the daily scale to facilitate comparisons with rain gauges. These two products here refer to the corresponding adjusted estimates based on the GPCC gauge network. We disaggregated the original 3B42 product (will be referred to as "3B42r"), with a gridbox resolution of 0.25° × 0.25°, into the same gridbox frame as the original IMERG product (with a gridbox resolution of 0.1° × 0.1°). We also aggregated the original IMERG product (will be referred to as "IMERGr") into the same grid frame as the original 3B42 product. Interpolating 3B42 from 0.25° × 0.25° to 0.1° × 0.1° may not be able to describe the higher rain rates and variability in finer resolutions. We used this disaggregated product only for a benchmark comparison on the original IMERG grid boxes. The disaggregation/aggregation strategies were implemented based on a distance-weighted average of the four nearest input grid boxes. The rainfall products were then intercompared in two separate groups: IMERG/3B42r and IMERGr/3B42.

Previous studies have reported that TRMM products perform poorly in winter months because of the presence of snow (Condom et al. 2011; Chen et al. 2013). It is also

well known that snowfall causes erroneous records in rain gauges, especially when snowfall constitutes a large portion of precipitation (Legates and Willmott 1990). We thus excluded the winter months from our study [see also Yin et al. (2008)], focusing on two rainy seasons (from 1 May to 31 October) over 2014 and 2015. Considering that peak streamflow mainly occurs during the rainy season in this region, it is critical to evaluate the utilities of IMERG and 3B42 products in driving hydrological simulations during this period.

3. Methodology

a. Statistical comparisons of satellite rainfall products against gauge observations

Rainfall estimates at satellite grid boxes with at least one rain gauge were compared with the gauged rainfall value within the grid box. Overall, 393 IMERG grid boxes and 169 3B42 grid boxes contain at least one rain gauge over the entire basin. Several widely used statistical metrics were applied to quantify the performance of the satellite rainfall products (Table 1; see also Yong et al. 2010): probability of detection (POD) assesses how well the satellite estimates detect the occurrence of rain events (daily rainfall accumulation greater than zero), frequency of hit (FOH) measures how often the satellite products detect rainfall when there is actually rainfall, false alarm ratio (FAR) measures how often the satellite products detect rainfall when there is actually no rainfall, critical success index (CSI) measures the fraction of satellite rain events that are correctly predicted, and Heidke skill score (HSS) measures the accuracy of the rainfall estimates considering matches due to random chance. All of these indices were calculated based on a contingency table (see Table 1; Mashingia et al. 2014). Additionally, a relative bias was adopted to measure the systematic difference between satellite and gauged rainfall accumulations. The coefficient of determination (RR) was used to measure the consistency between time series of satellite and gauged rainfall data.

b. Intercomparison of capture capability of rainfall variability in local domains

We evaluated satellite rainfall products in selected densely gauged local domains (consisting of four 3B42 grid boxes, with at least 10 gauges, and each 3B42 grid box is gauged). Considering that the original spatial resolutions of the 3B42 and IMERG products are 0.25° × 0.25° and 0.1° × 0.1°, respectively, every local domain correspondingly contains 25 IMERG grid boxes. To ensure each gridbox rainfall value can be compared with a referenced gauged rainfall value, only IMERG grid boxes that contain rain gauges were selected for the evaluation, whereas other grid boxes without rain gauges

TABLE 1. List of the statistical metrics used to quantify the performance of the satellite rainfall estimates (Mashingia et al. 2014). Note that S_i is the daily rainfall estimated by satellite products, G_i is the gauged daily rainfall, n is the total number of evaluated rain events obtained by timing the number of evaluated gauge station with the days in the study period, $\overline{S}/\overline{G}$ are the mean rainfall estimates generated by satellite/gauges over all the evaluated daily rain events, m is the number of rain gauges in each local domain, and t is the total number of days spanning the study period.

Statistical index	Equation	Perfect value
POD	$\dfrac{N_{11}}{N_{11} + N_{01}}$	1
FOH	$\dfrac{N_{11}}{N_{11} + N_{10}}$	1
FAR	$\dfrac{N}{N_{11} + N_{10}}$	0
CSI	$\dfrac{N_{11}}{N_{11} + N_{01} + N_{10}}$	1
HSS	$\dfrac{2(N_{11} - N_{00} - N_{10}N_{01})}{(N_{11} + N_{01})(N_{01} + N_{00}) + (N_{11} + N_{10})(N_{10} + N_{00})}$	1
N_{11}	Satellite is >0 and gauge is >0	
N_{10}	Satellite is >0 and gauge equals 0	
N_{01}	Satellite equals 0 and gauge is >0	
N_{00}	Satellite equals 0 and gauge equals 0	
Bias (%)	$100 \times \dfrac{\sum_{i=1}^{n}(S_i - G_i)}{\sum_{i=1}^{n} G_i}$	0
RR	$\dfrac{\left[\sum_{i=1}^{n}(S_i - \overline{S})(G_i - \overline{G})\right]^2}{\sum_{i=1}^{n}(S_i - \overline{S})^2 \sum_{i=1}^{n}(G_i - \overline{G})^2}$	1
BE (%)	$100 \times \dfrac{\sum_{i=1}^{t}[\min(S_i^1, \ldots, S_i^m) - \min(G_i^1, \ldots, G_i^m)]}{\sum_{i=1}^{t}[\min(G_i^1, \ldots, G_i^m)]}$	0

in each domain were simply discarded. Therefore, rainfall variability derived by the IMERG gridbox values was compared with the real rainfall variability derived by rain gauges in the identical measurement area. Figure 1c shows an example of a selected "local domain." It should be noted that the satellite gridbox rainfall value was repeated for multiple rain gauges within the same satellite grid box for the evaluation.

The representations of spatial rainfall variability within each "local domain" by satellite rainfall products were first measured by the bias values of the estimates (BE) of minimum daily rainfall (min), maximum daily rainfall (max), and the standard deviation of daily rainfall (std dev) [see also Liu (2015)]. Each statistical variable was calculated over all the evaluated grid boxes or gauges within each domain at the daily scale. Table 1 shows the equation used to compute the BE value for estimates of minimum daily rainfall (similar for maximum daily rainfall and standard deviation of daily rainfall). Additionally, the representations of spatial rainfall variability within each "local domain" were further measured by the detections in occurrence probabilities (OP) and amounts for different rain ranks.

We classified rainfall intensities into four categories (with six ranks): light-rain events, defined as 0–1 mm day^{-1}; moderate-rain events, defined as 1–5 and 5–10 mm day^{-1}; heavy-rain events, defined as 10–50 and 50–100 mm day^{-1}; and extreme heavy-rain events, defined as >100 mm day^{-1} [see also Tan et al. (2015) and Liu et al. (2015) for similar classification schemes]. The detection of OP was measured by the goodness of fit between the estimated and gauged OP for different rain ranks in the two rainy seasons, and the detection of rain amount was evaluated by the bias values obtained from satellite products for various rain ranks.

c. Hydrological evaluation of areal daily rainfall series

We further evaluated the utilities of IMERG and 3B42 rainfall products in hydrological simulations. The semi-distributed Xinanjiang (XAJ) model was adopted for this evaluation, which was first developed by Zhao (1992) and has been implemented successfully in a variety of hydrological settings (e.g., Tian et al. 2013; Zhuo et al. 2015), including cold mountainous basins such as the Tianshan in China (e.g., Jiang 1987; Mu and Jiang 2009).
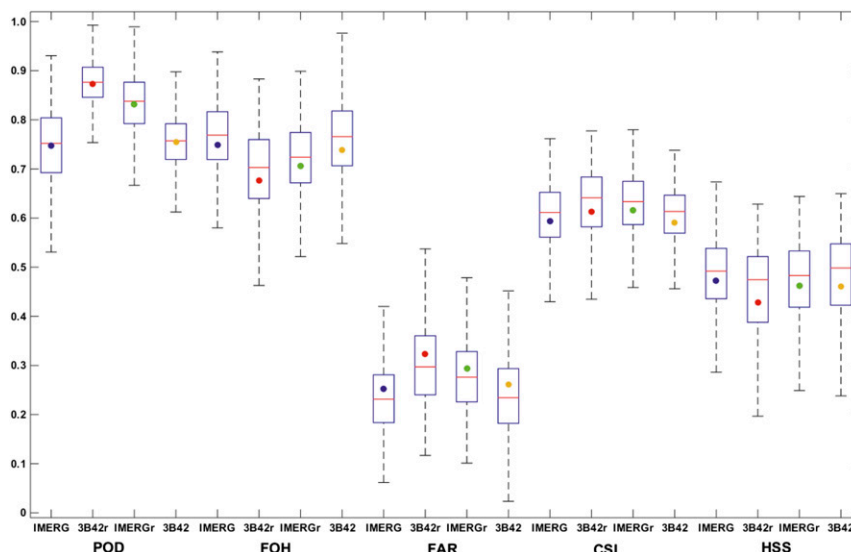
Fig. 2. Box plots of rainfall-detecting skill scores for the 503 rain gauges during the two rainy seasons.

The XAJ model adopts a tension water capacity curve to describe the nonuniform distribution of water capacity within a subcatchment. The tension water capacity curve is described by two parameters: spatial-averaged storage capacity and shape coefficient. The subcatchment tension water storage is conceptualized as the sum of tension water storages in the upper, lower, and deepest vertical layers, respectively. Overland runoff is generated by tension water storage release in the upper layer. The remainder of rainfall infiltrates and contributes to soil moisture and groundwater. Interflow and base flow are characterized by an exponential store (He et al. 2015). The model was calibrated during the rainy season of 2014 and then validated over the rainy season of 2015.

Three different parameter scenarios were designed to evaluate the performance of different rainfall inputs in hydrological simulation with the XAJ model (see also Sun et al. 2016; Tang et al. 2016b).

Scenario I: Model parameters were first calibrated using gauged rainfall data in the calibration period, and then the model was rerun using gauged rainfall data and the two satellite rainfall products in both of the calibration and validation periods. This calibration approach was designed to examine how IMERG and 3B42 products perform in streamflow simulation using gauge-calibrated parameters.

Scenario II: Model parameters were first calibrated using the 3B42 rainfall product in the calibration period, and then the model was rerun using gauged rainfall data and the two satellite rainfall products in both of the calibration and validation periods. This calibration scenario was used to investigate

how IMERG performs differently from 3B42 in streamflow simulation.

Scenario III: Model parameters were first calibrated using IMERG rainfall data in the calibration period, and then the model was rerun using gauged rainfall and the two satellite rainfall products in both of the calibration and validation periods. This scenario was adopted to complement the two aforementioned scenarios, considering the potential impact of uncertainty in rainfall inputs on model calibration.

The ε-Nondominated Sorting Genetic Algorithm II (ε-NSGAII) was used to automatically calibrate the model parameters (Deb et al. 2002; Kollat and Reed 2006). The objective function was to minimize the difference between the simulated and observed hydrographs at the outlet [or maximize the value of Nash–Sutcliffe efficiency coefficient (NSE); Nash and Sutcliffe 1970].

4. Results

a. Evaluation of rainfall products over the entire basin

Figure 2 shows the box plots of rainfall-detecting skill scores, including POD, FOH, FAR, CSI, and HSS. In the $0.1° \times 0.1°$ group, IMERG outperforms 3B42r with respect to three indices, FOH, FAR, and HSS, indicating that IMERG yields a higher frequency of successful hits when rainfall really occurs and a lower erroneous detection rate when there is actually no rainfall. In the $0.25° \times 0.25°$ group, IMERGr outperforms 3B42 with respect to three indices, POD, CSI, and HSS. An intercomparison between the two groups shows that the disaggregated/aggregated rainfall
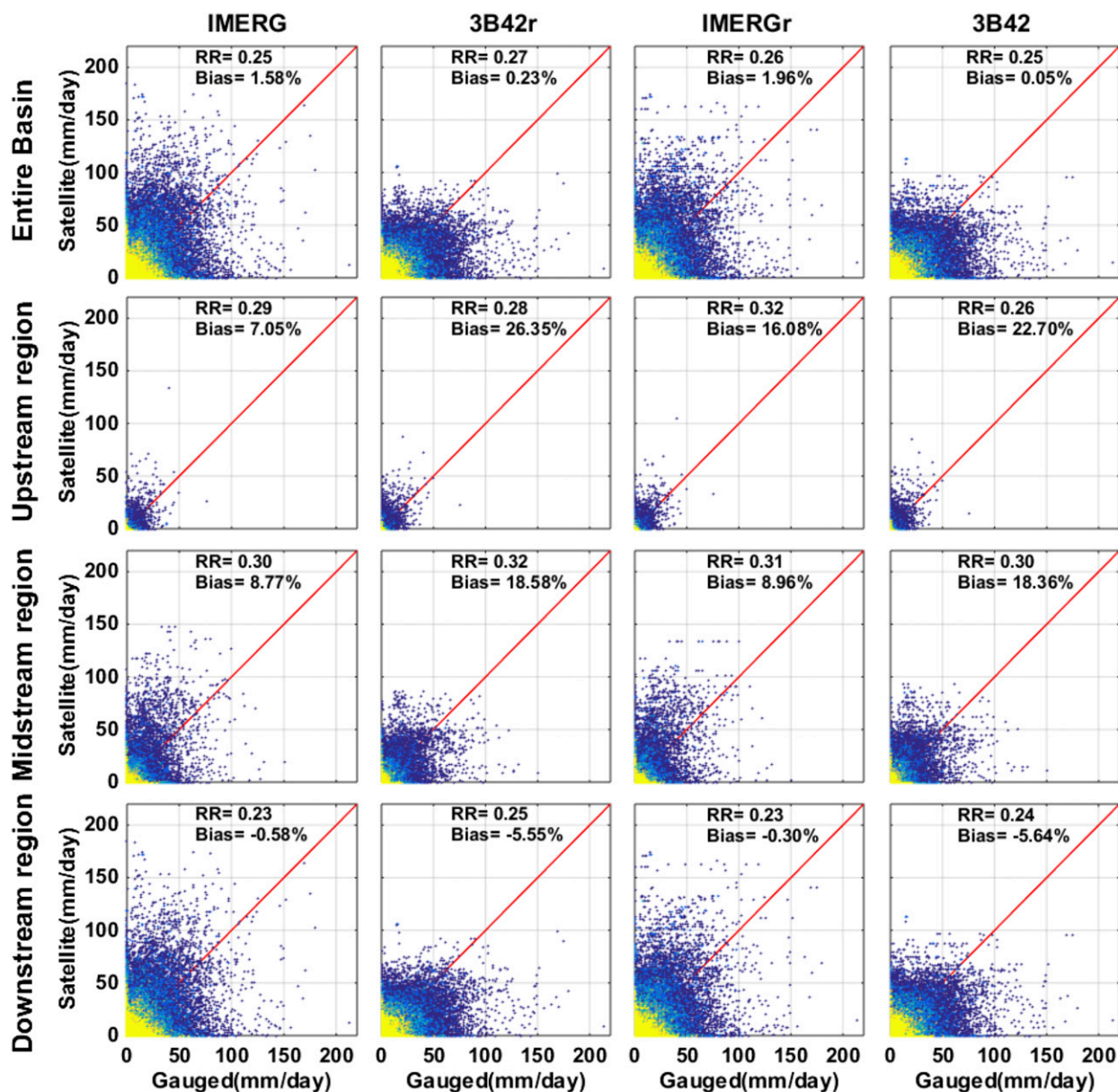
FIG. 3. Intercomparisons of daily rainfall intensities between rain gauges and satellite rainfall estimates during the two rainy seasons.

products tend to produce more frequent false alarms in rainfall estimates compared with the corresponding original rainfall products, potentially due to the overestimation of rain occurrence produced by the weighted average–based disaggregation/aggregation procedures.

Figure 3 shows the density-plot scatter diagrams of daily rainfall derived by various rainfall products. In the $0.1° \times 0.1°$ group, the differences between the RR values estimated by IMERG and 3B42r are consistently small across the entire basin, whereas the differences between bias values differ from the upstream region to the downstream region. The 3B42r shows smaller bias

values over the entire basin but much larger bias values in the upstream, midstream, and downstream regions compared with IMERG. It is noted that both of the two satellite products present positive bias values in the upstream and midstream regions but negative bias values in the downstream region. The offset effect between the positive and negative bias values in subregions leads to the smaller bias value for 3B42r over the entire basin. Results are extremely similar in the $0.25° \times 0.25°$ group (including IMERGr and 3B42 products).

Figure 4 and Table 2 summarize the bias value for each rain gauge produced by various satellite products.
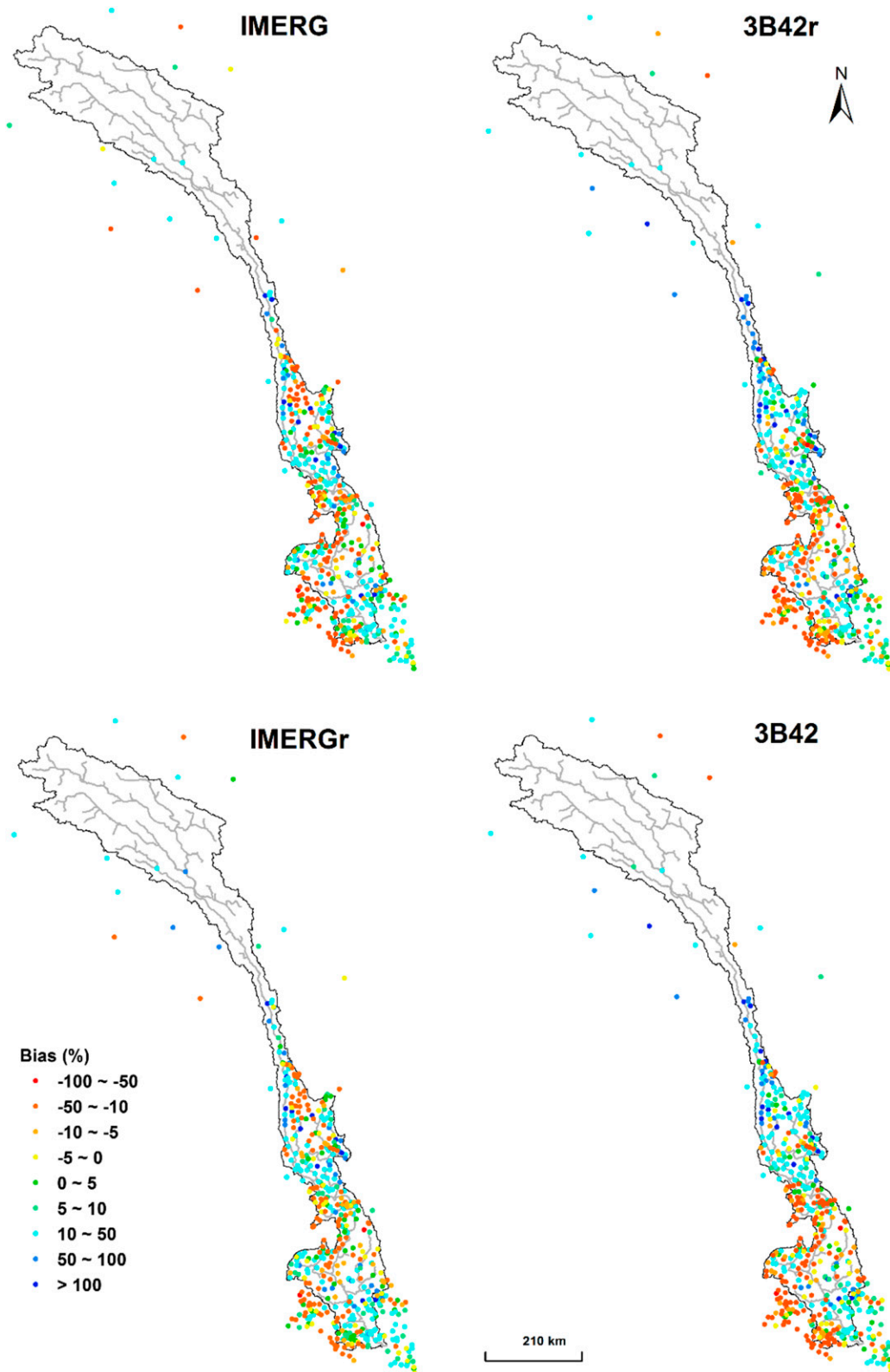
FIG. 4. Spatial distribution of the bias values for total rain amount in the two rainy seasons.

TABLE 2. Statistical summary of rainfall products performance in Figs. 4, 7, and 8. The number of gauges that obtained positive and negative bias values is indicated by NOG and NUG, respectively, during the two seasons. The number of gauges that obtained lower bias values for the corresponding dataset compared with the other rain dataset possessing the same spatial resolution is represented by NBG. Finally, the number of local domains that obtained better performance for rain occurrence probability/accumulation for the corresponding dataset compared with the other rain dataset possessing the same spatial resolution is indicated by NBDp/NBDa.

	IMERG	3B42r	IMERGr	3B42
Upstream				
NOG	11	15	14	15
NUG	7	3	4	3
NBG	10	8	11	7
Midstream				
NOG	102	128	104	131
NUG	60	34	58	31
NBG	90	72	85	77
Downstream				
NOG	179	129	179	135
NUG	144	194	144	188
NBG	187	136	181	142
	Total (NOG/NUG/NBG)			
	292/211/287	272/231/216	297/206/277	281/222/226
0–1 mm day^{-1} NBDp/NBDa	15/8	5/12	11/0	9/20
1–5 mm day^{-1} NBDp/NBDa	16/18	4/2	11/11	9/9
5–10 mm day^{-1} NBDp/NBDa	17/18	3/2	15/16	5/4
10–50 mm day^{-1} NBDp/NBDa	8/8	12/12	8/8	12/12
50–100 mm day^{-1} NBDp/NBDa	10/10	10/10	10/10	10/10
>100 mm day^{-1} NBDp/NBDa	15/15	2/2	15/15	1/1

We found that positive bias values prevail in the upstream and midstream regions for both of the IMERG and 3B42r products (NOG > NUG, Table 2). In the downstream region, positive bias values still prevail for IMERG, whereas negative bias values prevail for 3B42r. NBG in Table 2 presents the number of gauges that obtained smaller bias values for the corresponding product compared with the other product with the same gridbox scale and indicates that IMERG outperforms 3B42r on most of the rain gauges. A comparison between IMERGr and 3B42 reveals a similar situation. The spatial distributions of bias values obtained by IMERG and 3B42r could be related to the topographic features and distribution of rainfall accumulations over the basin. The terrain varies significantly over the midstream region, which would exert a

strong topographic effect on rainfall processes (e.g., Giovannettone and Barros 2009). Comparisons for this region indicate that IMERG tends to capture the topographic effect on rainfall better than 3B42r. In the downstream region, rainfall accumulation is much higher than those in the midstream and upstream regions. IMERG tends to capture the rain amount better than 3B42r on gauges with higher rainfall accumulations (see NBG in Table 2). Differences in intrinsic characteristics, such as rainfall retrieval algorithms and sensors used, between satellite datasets should potentially contribute to the differences in performance of satellite rainfall products across rain gauges.

To explore the dependence of product performance on rainfall accumulation, we further evaluated the relationship between rain product performance and mean gauged daily rainfall during the two rainy seasons on each gauge (Fig. 5). As expected, RR values decrease with an increase in mean gauged daily rainfall, showing significant trends (Fig. 5a). This could be attributed to the fact that frequent rain events on wet gauges may increase the possibility of miss representation in satellite products. The results indicate that the consistency between the satellite and gauged rainfall time series tends to be lower on wetter gauges. However, with respect to the bias values, the dependence of product performance on rainfall accumulation differs between dry and wet gauges. Figure 5b shows that the bias presents primarily positive values on gauges with a mean gauged daily rainfall lower than 4.5 mm day^{-1}, whereas it shows predominantly negative values on gauges with mean gauged daily rainfall above this threshold. An intercomparison of RR values obtained by IMERG and 3B42r indicates that there is no significant trend between the RR difference (ΔRR) and mean gauged daily rainfall (Figs. 5c,e). Regarding the bias values (Figs. 5d,f), there is a threshold of mean gauged daily rainfall (around 4.5 mm day^{-1}), below which IMERG outperforms 3B42r, and the improvement obtained by IMERG decreases with the increase in the mean gauged daily rainfall. For gauges where mean gauged daily rainfall exceeds that threshold, IMERG outperforms 3B42r with an increasing trend when mean gauged daily rainfall is increasing. Products in the 0.25° × 0.25° group (including IMERGr and 3B42 products) show highly similar trends and will not be elaborated. Results indicate that IMERG tends to outperform 3B42 more significantly on extreme wet/dry gauges, which should be attributed to the intrinsic characteristics of the retrieval algorithms and sensors used.

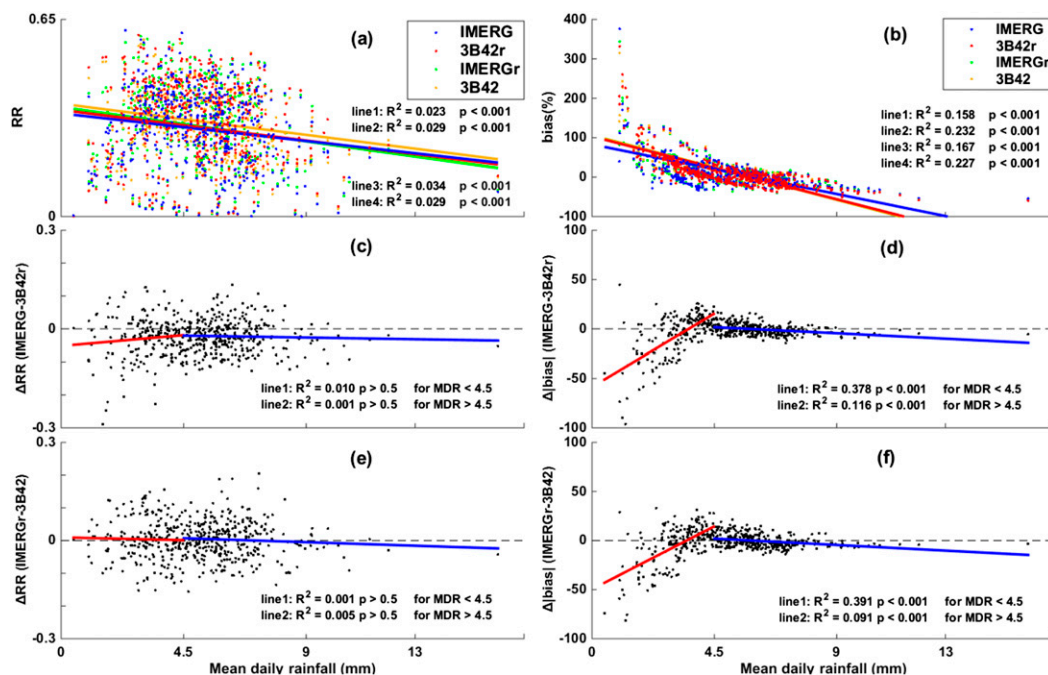Figure 6 compares the spatial patterns of mean daily rainfall estimated by various datasets over the two rainy

FIG. 5. Relationships between satellite products performance and mean daily rainfall on gauges.

seasons. Rainfall patterns of gauge data were obtained by interpolating point rain gauges via the inverse distance weighting scheme. In the downstream region, IMERG captures heavy-rainfall areas better than 3B42, especially for the heavy-rainfall areas on the southwestern boundary of the basin. In the midstream region, the IMERG patterns are also more similar to the gauged patterns and show higher spatial variability than those derived from 3B42r. Because of the limited number of rain gauges in the upstream region, we are not able to determine which rainfall product is better than the other one. However, it is noteworthy that IMERG patterns show much higher spatial variability than those derived from 3B42r. Differences in rainfall patterns obtained by IMERG and 3B42r should again be related to the topographic features and distribution of rainfall accumulations over the basin. A comparison between IMERGr and 3B42 patterns yields similar results.

b. Detection of rainfall variability within local domains

Twenty "local domains" were selected over the entire basin (see Fig. 1b for locations), which are mainly located in the midstream and downstream regions. Table 3 presents the BE values for the minimum, maximum, and standard deviation of daily rainfall during the two rainy seasons, as well as the numbers of evaluated rain gauges and the IMERG grid boxes in each domain. For the

minimum daily rainfall, all of the satellite products exhibited overestimation over all local domains. The maximum and standard deviation of daily rainfall were systematically underestimated by all of the satellite products. However, it is noteworthy that IMERG (IMERGr) tends to yield smaller BE values for all of the three statistical variables than 3B42r (3B42) in all local domains, indicating a higher ability to capture the spatial rainfall variability.

We further compared the abilities of the rainfall products in reproducing the occurrence probabilities and accumulations of rain events with different intensities. IMERG tends to overestimate the occurrence probability of rainfall with an intensity of 0–1 mm day^{-1}, whereas 3B42r tends to underestimate the occurrence probability of these rain events (Fig. 7). Regarding the rain events falling into the 1–5 mm day^{-1} category, detections of various rain datasets are similar and tend to match the gauged results well. For the rain events with an intensity of 5–50 mm day^{-1}, IMERG underestimates the probability of rain occurrence, whereas 3B42r overestimates the probability of rain occurrence in more than 10 local domains. For rain ranks higher than 50 mm day^{-1}, IMERG overestimates the rain occurrence probability, whereas 3B42r underestimates the rain occurrence probability. Overall, for rain ranks lower than 10 mm day^{-1} and higher than 100 mm day^{-1}, IMERG agrees with the rain gauges better than 3B42r does in most local domains, whereas for rain
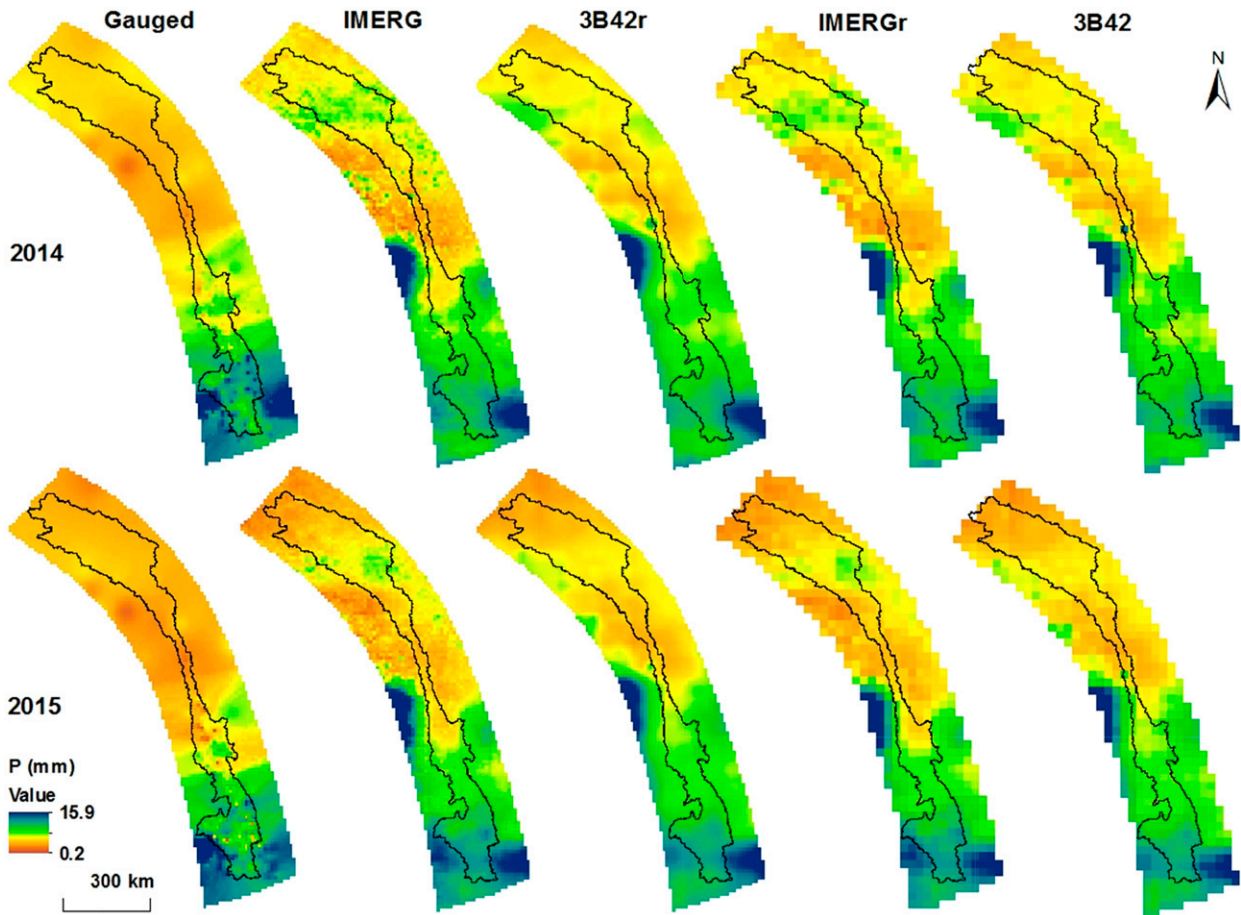
FIG. 6. Rainfall patterns represented by mean daily rainfall. Shown are the patterns in the (top) 2014 and (bottom) 2015 rainy seasons.

rank falling into the 10–50 mm day^{-1} category, 3B42r tends to outperform IMERG in most local domains (see NBDp values in Table 2). Comparisons between IMERGr and 3B42 yield similar results (figure not shown).

Figure 8 shows that IMERG tends to overestimate the amounts of rain events lower than 5 mm day^{-1} and rain events higher than 50 mm day^{-1} but underestimate the amounts of rain ranks falling into the 5–50 mm day^{-1} category, whereas the opposites tend to be true for 3B42r, apart from the similar overestimation for 0–5 mm day^{-1} rain events obtained by 3B42r. In terms of the absolute bias values (see also NBDa in Table 2), IMERG outperforms 3B42r on rain ranks of 1–5, 5–10, and >100 mm day^{-1}, but not on rain ranks of 0–1, 10–50, and 50–100 mm day^{-1}. It is noted that 3B42r fails to detect extreme heavy-rain events (>100 mm day^{-1}) in all local domains, whereas IMERG does present these rain events, even though the corresponding rain amounts tend to be overestimated.

Overall, significant differences between the IMERG (IMERGr) and 3B42r (3B42) products mainly occur with

respect to the detections of occurrence probabilities and amounts for extreme rain events, that is, 0–1 mm day^{-1} and >100 mm day^{-1}. The differences in the performance of the satellite rainfall products over various rain ranks could be attributed to differences in rainfall retrieval methods as well as the satellite sensors used in the two products (Huffman and Bolvin 2015). The IMERG *Core Observatory* helps to extend the measurement range attained by TRMM and contributes to the better performance of IMERG in reproducing the occurrence probabilities of light- and heavy-rain events. However, the rain amounts derived by the IMERG retrieval algorithm significantly overestimate the light- and heavy-rain accumulations.

c. Comparison of performance in hydrological simulation

We applied the semidistributed XAJ model over the upstream region of UMRB, with a total drainage area of 78 277 km^2 (total discharge is gauged by the Changdu hydrologic station; see its location in Fig. 1a). We chose the upstream region of the basin as our test bed simply

TABLE 3. Bias values for estimates (100%) of statistical variables of daily rainfall (including min, max, and std dev) by satellite products in 20 local domains.

No. of domain	No. of gauge	No. of IMERG grid box	Min				Max				Std dev			
			IMERG	3B42r	IMERGr	3B42	IMERG	3B42r	IMERGr	3B42	IMERG	3B42r	IMERGr	3B42
1	16	14	13.27	26.28	16.01	26.45	−0.20	−0.29	−0.29	−0.30	−0.33	−0.55	−0.37	−0.41
2	10	9	2.11	6.35	3.52	6.53	−0.22	−0.33	−0.33	−0.35	−0.29	−0.55	−0.46	−0.48
3	13	11	1.74	5.31	2.73	5.74	−0.34	−0.36	−0.47	−0.40	−0.37	−0.51	−0.51	−0.47
4	11	10	3.36	8.48	4.69	8.65	−0.07	−0.22	−0.18	−0.25	−0.19	−0.50	−0.29	−0.48
5	10	9	2.14	5.05	2.68	5.32	−0.26	−0.33	−0.35	−0.37	−0.35	−0.55	−0.41	−0.48
6	12	14	17.33	21.32	23.15	21.90	−0.42	−0.52	−0.56	−0.52	−0.53	−0.64	−0.63	−0.59
7	15	13	7.80	10.93	8.42	11.51	−0.28	−0.42	−0.37	−0.44	−0.40	−0.59	−0.50	−0.55
8	22	15	17.94	22.95	23.76	20.61	−0.44	−0.57	−0.54	−0.55	−0.51	−0.69	−0.60	−0.59
9	16	14	2.82	4.83	3.61	4.93	−0.38	−0.55	−0.46	−0.57	−0.45	−0.67	−0.53	−0.63
10	14	12	—	—	—	—	−0.41	−0.54	−0.49	−0.56	−0.51	−0.66	−0.57	−0.61
11	12	10	4.01	4.92	4.90	5.07	−0.43	−0.56	−0.52	−0.58	−0.49	−0.67	−0.59	−0.56
12	11	11	1.27	1.96	1.82	1.95	−0.35	−0.54	−0.44	−0.54	−0.40	−0.65	−0.51	−0.55
13	11	10	2.92	3.85	3.35	4.24	−0.47	−0.60	−0.53	−0.62	−0.49	−0.67	−0.54	−0.62
14	21	16	4.23	6.27	5.55	6.60	−0.34	−0.54	−0.46	−0.55	−0.38	−0.66	−0.49	−0.59
15	11	11	3.41	4.52	4.06	4.21	−0.47	−0.58	−0.53	−0.57	−0.57	−0.72	−0.62	−0.68
16	14	13	7.02	10.50	9.56	10.96	−0.48	−0.60	−0.57	−0.60	−0.55	−0.72	−0.61	−0.67
17	25	15	10.59	13.97	13.04	14.44	−0.49	−0.63	−0.57	−0.64	−0.57	−0.73	−0.64	−0.71
18	17	12	4.44	5.53	5.81	5.32	−0.51	−0.64	−0.60	−0.64	−0.57	−0.73	−0.65	−0.65
19	27	16	57.79	74.95	61.32	73.64	−0.45	−0.55	−0.48	−0.56	−0.58	−0.72	−0.59	−0.69
20	12	10	7.39	8.97	8.50	9.73	−0.44	−0.57	−0.51	−0.59	−0.53	−0.68	−0.57	−0.65
Mean	15	12	9.03	13.00	10.87	13.04	−0.37	−0.50	−0.46	−0.51	−0.45	−0.64	−0.53	−0.58

because the stream is less affected by anthropogenic regulation (e.g., hydropower generation). An inverse distance interpolation method was used to derive areal rainfall from rain gauges. For the satellite rainfall products, we used 3B42 and IMERG only.

Figure 9 shows the hydrological simulations under three parameter scenarios in both of the calibration and validation periods. The corresponding simulated NSE values are presented in Table 4. For scenario I, the NSE obtained by gauge data in the calibration period reached 0.63 but was negative in the validation period. Using the gauge-calibrated parameter set for IMERG and 3B42 products, streamflow simulations performed worse than those driven by gauge data in both of the calibration and validation periods. Overall, both of the IMERG and 3B42 products produced significant overestimation in the simulated streamflow time series.

Under parameter scenario II, 3B42 data produced an NSE value of 0.65 in the calibration period but a negative value in the validation period. Forced by gauge data, the model clearly underestimated the streamflow time series in both of the calibration and validation periods, particularly for peak flows, indicating a much lower rainfall accumulation in the sparse gauged input. Forcing the model by IMERG data, the NSE value was 0.63 in the calibration period, close to that obtained by 3B42 data, but was also negative in the validation period. Figure 9b indicates a sound agreement between the 3B42- and IMERG-driven hydrographs when using the 3B42-calibrated parameters, apart from the much larger overestimation in peak flows produced by IMERG.

When using parameters from scenario III, IMERG obtained NSE values of 0.76 and 0.53 in the calibration and validation periods, respectively. Driving the model by gauge data, streamflow time series were clearly underestimated, similarly to those in scenario II. The NSE values produced by 3B42 were 0.64 and 0.49 in the calibration and validation periods, respectively, indicating simulations comparable to those of IMERG.

The areal average daily rainfall in Fig. 10a illustrates the dominances of different daily rain ranks with respect to various rainfall inputs. IMERG and rain gauge inputs are characterized by the largest rainfall accumulation from 2 to 5 mm day^{-1} events, whereas 3B42 input is characterized by the largest rainfall accumulation from 5 to 8 mm day^{-1} events. It is noted that only IMERG contains rain events with intensity higher than 20 mm day^{-1}. In general, IMERG contains the largest input rainfall accumulation, followed by 3B42. Simulated bias values for ranked streamflow observations during both of the calibration and validation periods were investigated in Figs. 10b–d. We ranked the streamflow events into seven quantiles, that is, 5, 10, 25, 50, 75, 90, and 95 quantiles, in the combined streamflow time series. When using the gauge-calibrated parameters in scenario I, both of the IMERG and 3B42 products significantly overestimated
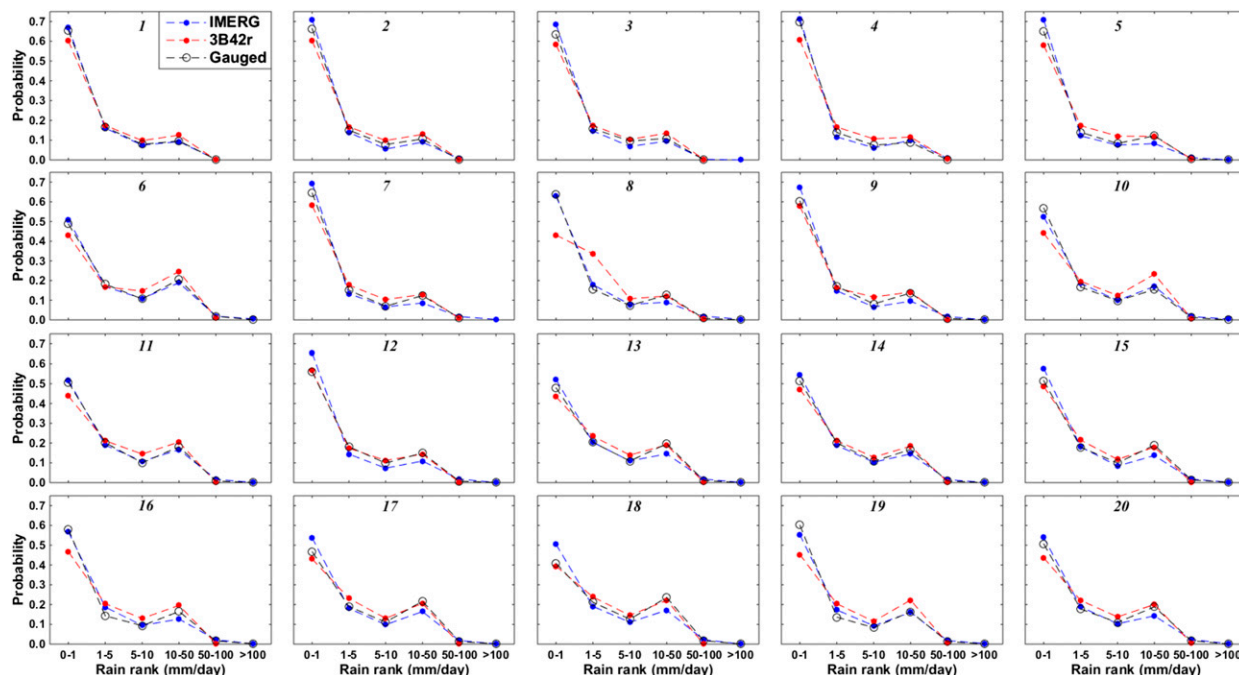
FIG. 7. Comparisons of the occurrence probabilities of six rain ranks detected by satellite products in twenty local domains.

all of the streamflow ranks. Bias patterns in scenario II show that IMERG produced larger bias values for moderate flows but smaller bias values for low and peak flows compared with 3B42, whereas IMERG outperformed 3B42 on all of the streamflow ranks in scenario III.

Overall, simulations in scenarios I and II indicate that IMERG and 3B42 mainly produce different simulations for extreme streamflow events, which is consistent with the results of statistical comparisons discussed in previous subsections. Results in scenarios
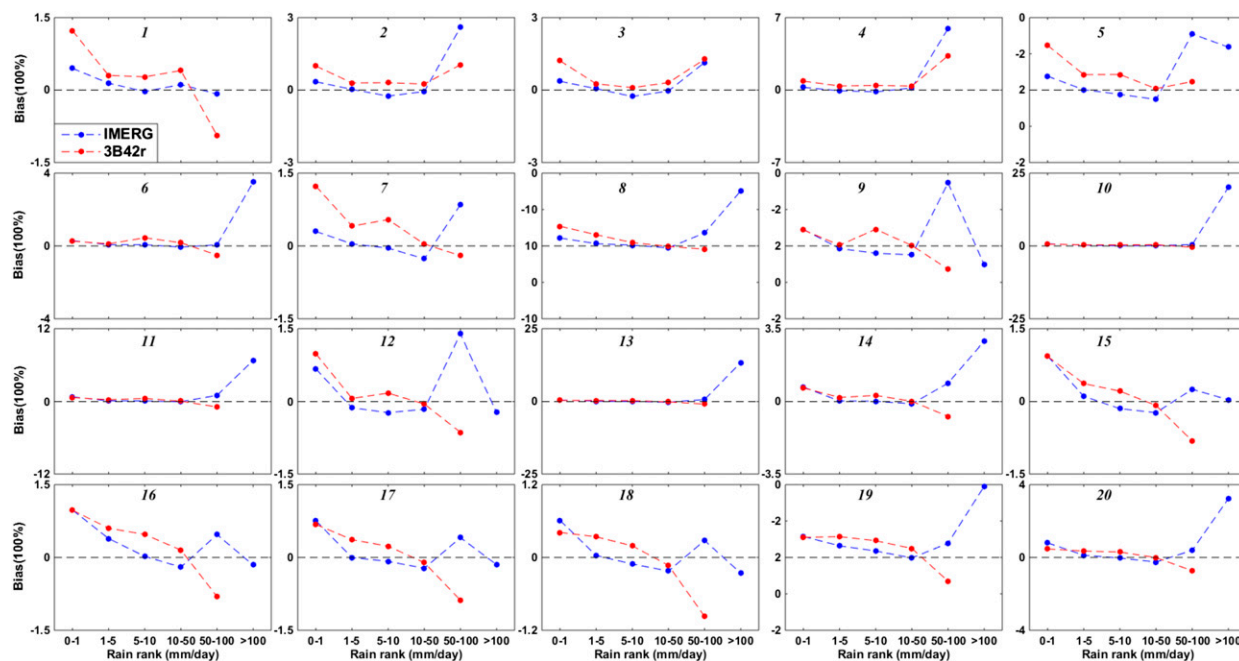

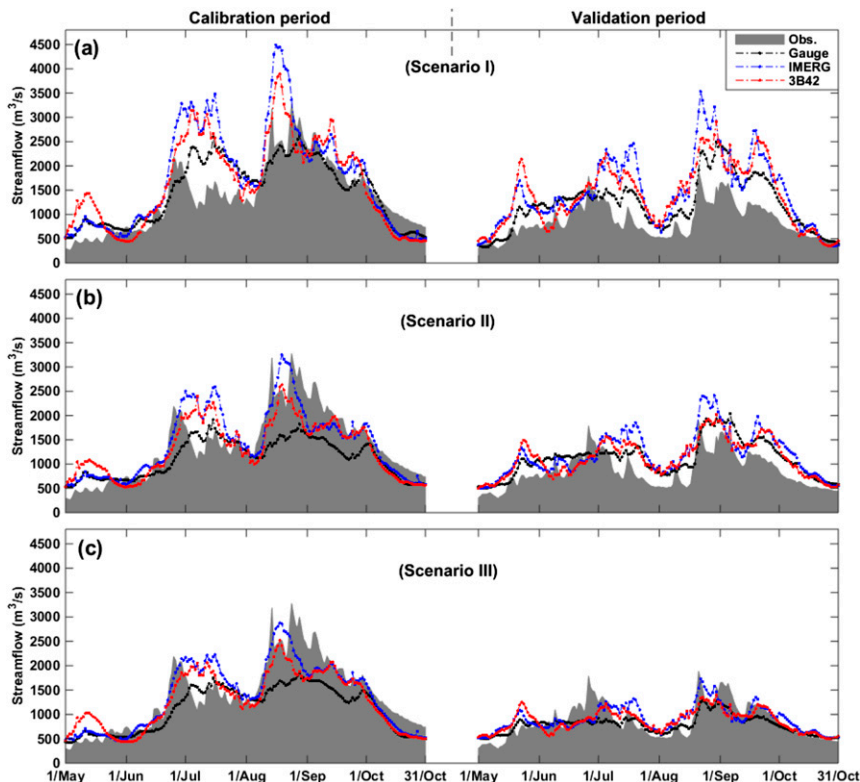FIG. 8. As in Fig. 7, but for the bias values of amounts of six rain ranks.

FIG. 9. Streamflow simulations using different rain inputs under three parameter scenarios in the upstream region of the UMRB.

II and III clearly demonstrate sound agreement in hydrological simulations driven by 3B42 and IMERG, which tends to be independent of the calibrated parameters. Moreover, simulations in three parameter scenarios reveal that IMERG outperforms 3B42 and sparse gauge data when calibrating model parameters using each rainfall input.

5. Summary and conclusions

In this study, we performed an early quantitative evaluation of error characteristics of IMERG product for daily rainfall estimates in a mountainous basin. The IMERG was also intercompared with its predecessor, the TRMM 3B42V7 product. We examined the dependences of the two satellite rainfall products' performance on daily rainfall intensities and investigated their utilities in driving hydrological simulations. Our study provides unique insights by focusing on a mountainous region with an exceptionally dense rain gauge network. The main results are summarized as follows.

1) The IMERG product tends to produce systematically lower bias values for daily rainfall estimates and indeed outperforms the 3B42 product in capturing

spatial rainfall variability and the estimates of moderate-rain events with an intensity of 1–10 mm day^{-1}.

2) There are strong dependences on rainfall intensities for the performance of both of the IMERG and 3B42 rainfall estimates. For rain ranks lower than 10 mm day^{-1} and higher than 100 mm day^{-1}, IMERG detects rain occurrence probability better than 3B42r does, whereas for rain rank falling into the 10–50 mm day^{-1} category, 3B42r tends to outperform IMERG. IMERG outperforms 3B42r on rain ranks of 1–5, 5–10, and >100 mm day^{-1} but not on rain ranks of 0–1, 10–50, and 50–100 mm day^{-1} for the estimates of rain amount. The different performances

TABLE 4. NSE values of streamflow simulations driven by various rainfall products, that is, gauge, IMERG, and 3B42, in three parameter scenarios.

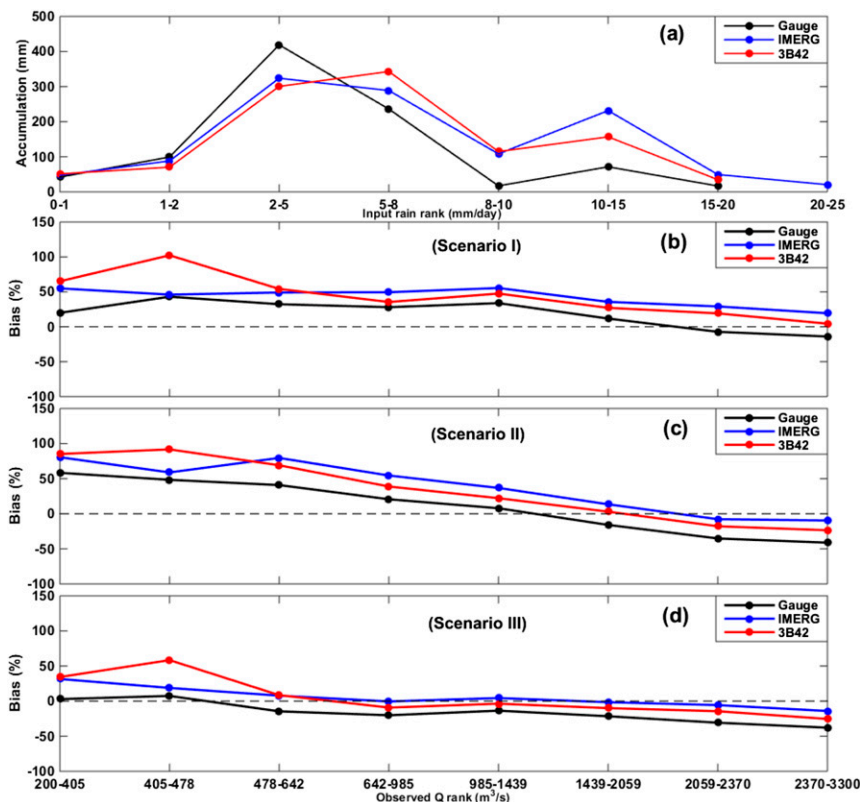|	Calibration period			Validation period		
	Gauge	IMERG	3B42	Gauge	IMERG	3B42
Scenario I	0.63	−0.19	0.18	−0.28	−3.09	−2.55
Scenario II	0.44	0.63	0.65	0.31	−0.60	−0.06
Scenario III	0.54	0.76	0.64	0.43	0.53	0.49

FIG. 10. Comparisons of various rain inputs for hydrological modeling in the upstream region of UMRB, and simulated bias values for various streamflow ranks by three different rain inputs.

observed for different rainfall intensities could be attributed to the intrinsic features of the two satellite products produced by algorithmic and sensor discrepancies. Benefiting from advanced satellite sensors, IMERG detects the occurrences of light-rain and extreme heavy-rain ranks better than 3B42 does. However, the IMERG algorithm tends to produce significant overestimation of the amounts of extreme rain events.

3) Streamflow simulations performed under three different parameter scenarios show that IMERG generally produces simulations comparable to those produced by 3B42. IMERG tends to be able to "fill the gaps" in driving hydrological models well after the TRMM-era product. This result provides a basis for the further application of upcoming retrospectively generated IMERG product using TRMM products. Additionally, IMERG tends to outperform 3B42 when calibrating model parameters with each rainfall dataset, indicating the promising utility of IMERG for driving hydrological models in mountainous basins where the rain gauge network is sparse.

To make the gridbox resolutions identical, we disaggregated the original 3B42 product into one with a resolution of 0.1° × 0.1°, the same resolution as the original IMERG, in the first group. In the second group, we aggregated the original IMERG product into one with a resolution of 0.25° × 0.25°, the same resolution of the original 3B42. Our results show that the gridbox size has significant effects on the gridbox rainfall values. However, intercomparisons of satellite products in the two groups yielded the extremely similar results, indicating that our aforementioned findings are not subject to the gridbox scale.

Even though our evaluation is based on a 2-yr dataset, we believe the performance of IMERG rainfall estimates as revealed by the recently released product could provide timely and useful implications on the improvement of rainfall retrieval algorithm. At the earlier stage of TRMM rainfall products, improvement of the TMPA retrieval algorithm also benefited from vast timely ground validations (e.g., Wolff et al. 2005; Shige et al. 2006; Seto et al. 2011). Some of these early studies provided useful information pertaining to the error characteristics of original TRMM products based on a short time series (e.g., Barros et al.

2000; Negri et al. 2002; Harris et al. 2007). Our findings regarding the differences between IMERG and 3B42 products could provide useful feedback for IMERG algorithm developers for potential improvement.

Our results show that integrating new satellite sensors and algorithms leads to mixed performance regarding various rainfall intensities by IMERG. We believe that our results could be further validated by a future comparison between retrospectively generated IMERG products and TRMM products and contribute to differentiating algorithmic and satellite sensor differences.

REFERENCES

Barros, A. P., M. Joshi, J. Putkonen, and D. W. Burbank, 2000: A study of the 1999 monsoon rainfall in a mountainous region in central Nepal using TRMM products and rain gauge observations. *Geophys. Res. Lett.*, **27**, 3683–3686, doi:10.1029/2000GL011827.

——, and Coauthors, 2014: NASA GPM-Ground Validation: Integrated Precipitation and Hydrology Experiment 2014 science plan. NASA, 66 pp. [Available online at https://pmm.nasa.gov/iphex.]

Brutsaert, W., 2005: *Hydrology: An Introduction.* Cambridge University Press, 605 pp.

Castro, L. M., M. Miranda, and B. Fernandez, 2015: Evaluation of TRMM Multi-satellite Precipitation Analysis (TMPA) in a mountainous region of the central Andes range with a Mediterranean climate. *Hydrol. Res.*, **46**, 89–105, doi:10.2166/nh.2013.096.

Chen, S., and Coauthors, 2013: Evaluation of the successive V6 and V7 TRMM Multisatellite Precipitation Analysis over the continental United States. *Water Resour. Res.*, **49**, 8174–8186, doi:10.1002/2012WR012795.

Condom, T., P. Rau, and J. C. Espinoza, 2011: Correction of TRMM 3B43 monthly precipitation data over the mountainous areas of Peru during the period 1998–2007. *Hydrol. Processes*, **25**, 1924–1933, doi:10.1002/hyp.7949.

Deb, K., A. Pratap, S. Agarwal, and T. Meyarivan, 2002: A fast and elitist multiobjective genetic algorithm: NSGA-II. *IEEE Trans. Evol. Comput.*, **6**, 182–197, doi:10.1109/4235.996017.

Dinku, T., P. Ceccato, E. Grover-Kopec, M. Lemma, S. J. Connor, and C. F. Ropelewski, 2007: Validation of satellite rainfall products over East Africa's complex topography. *Int. J. Remote Sens.*, **28**, 1503–1526, doi:10.1080/01431160600954688.

Giovannettone, J. P., and A. P. Barros, 2009: Probing regional orographic controls of precipitation and cloudiness in the central Andes using satellite data. *J. Hydrometeor.*, **10**, 167–182, doi:10.1175/2008JHM973.1.

Harris, A., S. Rahman, F. Hossain, L. Yarborough, A. C. Bagtzoglou, and G. Easson, 2007: Satellite-based flood modeling using TRMM-based rainfall products. *Sensors*, **7**, 3416–3427, doi:10.3390/s7123416.

He, Z. H., F. Q. Tian, H. V. Gupta, H. C. Hu, and H. P. Hu, 2015: Diagnostic calibration of a hydrological model in a mountain area by hydrograph partitioning. *Hydrol. Earth Syst. Sci.*, **19**, 1807–1826, doi:10.5194/hess-19-1807-2015.

——, H. C. Hu, F. Q. Tian, G. H. Ni, and Q. F. Hu, 2017: Correcting the TRMM rainfall product for hydrological modelling in sparsely-gauged mountainous basins. *Hydrol. Sci. J.*, **62**, 306–318, doi:10.1080/02626667.2016.1222532.

Hou, A. Y., G. Skofronick-Jackson, C. D. Kummerow, and J. M. Shepherd, 2008: Global Precipitation Measurement. *Precipitation: Advances in Measurement, Estimation and Prediction*, S. Michaelides, Ed., Springer, 131–169, doi:10.1007/978-3-540-77655-0_6.

——, and Coauthors, 2014: The Global Precipitation Measurement mission. *Bull. Amer. Meteor. Soc.*, **95**, 701–722, doi:10.1175/BAMS-D-13-00164.1.

Huffman, G. J., and D. T. Bolvin, 2015: TRMM and other data precipitation data set documentation. NASA TRMM Doc., 44 pp. [Available online at http://pmm.nasa.gov/sites/default/files/imce/3B42_3B43_doc_V7.pdf.]

——, and Coauthors, 2007: The TRMM Multisatellite Precipitation Analysis (TMPA): Quasi-global, multiyear, combined-sensor precipitation estimates at fine scales. *J. Hydrometeor.*, **8**, 38–55, doi:10.1175/JHM560.1.

Jiang, H. F., 1987: Snow ablation modeling and its application to Qiedeke basin (in Chinese). *J. Xinjiang Agric. Univ.*, **1**, 67–75.

Jiang, S. H., L. L. Ren, Y. Hong, B. Yong, X. L. Yang, F. Yuan, and M. W. Ma, 2012: Comprehensive evaluation of multi-satellite precipitation products with a dense rain gauge network and optimally merging their simulated hydrological flows using the Bayesian model averaging method. *J. Hydrol.*, **452–453**, 213–225, doi:10.1016/j.jhydrol.2012.05.055.

Joyce, R. J., J. E. Janowiak, P. A. Arkin, and P. P. Xie, 2004: CMORPH: A method that produces global precipitation estimates from passive microwave and infrared data at high spatial and temporal resolution. *J. Hydrometeor.*, **5**, 487–503, doi:10.1175/1525-7541(2004)005<0487:CAMTPG>2.0.CO;2.

Kidd, C., and G. Huffman, 2011: Global Precipitation Measurement. *Meteor. Appl.*, **18**, 334–353, doi:10.1002/met.284.

Kollat, J. B., and P. M. Reed, 2006: Comparing state-of-the-art evolutionary multi-objective algorithms for long-term groundwater monitoring design. *Adv. Water Resour.*, **29**, 792–807, doi:10.1016/j.advwatres.2005.07.010.

Krakauer, N. Y., S. M. Pradhanag, T. Lakhankar, and A. K. Jha, 2013: Evaluating satellite products for precipitation estimation in mountain regions: A case study for Nepal. *Remote Sens.*, **5**, 4107–4123, doi:10.3390/rs5084107.

Legates, D. R., and C. J. Willmott, 1990: Mean seasonal and spatial variability in gauge-corrected, global precipitation. *Int. J. Climatol.*, **10**, 111–127, doi:10.1002/joc.3370100202.

Liu, J. Z., Z. Duan, J. C. Jiang, and A. X. Zhu, 2015: Evaluation of three satellite precipitation products TRMM 3B42, CMORPH, and PERSIANN over a subtropical watershed in China. *Adv. Meteor.*, **2015**, 151239, doi:10.1155/2015/151239.

Liu, Z., 2015: Comparison of precipitation estimates between version 7 3-hourly TRMM Multi-satellite Precipitation Analysis (TMPA) near-real-time and research products. *Atmos. Res.*, **153**, 119–133, doi:10.1016/j.atmosres.2014.07.032.

——, 2016: Comparison of Integrated Multisatellite Retrievals for GPM (IMERG) and TRMM Multisatellite Precipitation Analysis (TMPA) monthly precipitation products: Initial results. *J. Hydrometeor.*, **17**, 777–790, doi:10.1175/JHM-D-15-0068.1.

Livneh, B., J. S. Deems, D. Schneider, J. J. Barsugli, and N. P. Molotch, 2014: Filling in the gaps: Inferring spatially distributed precipitation from gauge observations over complex terrain. *Water Resour. Res.*, **50**, 8589–8610, doi:10.1002/2014WR015442.

Manh, N. V., N. V. Dung, N. N. Hung, M. Kummu, B. Merz, and H. Apel, 2015: Future sediment dynamics in the Mekong Delta floodplains: Impacts of hydropower development, climate change and sea level rise. *Global Planet. Change*, **127**, 22–33, doi:10.1016/j.gloplacha.2015.01.001.

Mashingia, F., F. Mtalo, and M. Bruen, 2014: Validation of remotely sensed rainfall over major climatic regions in northeast Tanzania. *Phys. Chem. Earth*, **67–69**, 55–63, doi:10.1016/j.pce.2013.09.013.

Meng, J., L. Li, Z. C. Hao, J. H. Wang, and Q. X. Shao, 2014: Suitability of TRMM satellite rainfall in driving a distributed hydrological model in the source region of Yellow River. *J. Hydrol.*, **509**, 320–332, doi:10.1016/j.jhydrol.2013.11.049.

Mu, Z. X., and H. F. Jiang, 2009: Establishment of snowmelt type Xin'anjiang watershed model based on digital elevation model (in Chinese). *J. Xinjiang Agric. Univ.*, **5** (32), 75–80.

NASA, 2015: GPM/DPR level-3. Algorithm Theoretical Basis Doc., 12 pp. [Available online at https://pps.gsfc.nasa.gov/Documents/Level%203%20DPR%20ATBD.pdf.]

Nash, J. E., and J. V. Sutcliffe, 1970: River flow forecasting through conceptual models part I—A discussion of principles. *J. Hydrol.*, **10**, 282–290, doi:10.1016/0022-1694(70)90255-6.

Negri, A. J., R. F. Adler, and L. Xu, 2002: A TRMM-calibrated infrared rainfall algorithm applied over Brazil. *J. Geophys. Res.*, **107**, 8048, doi:10.1029/2000JD000265, 2002.

Prakash, S., A. K. Mitra, D. S. Pai, and A. AghaKouchak, 2016: From TRMM to GPM: How well can heavy rainfall be detected from space? *Adv. Water Resour.*, **88**, 1–7, doi:10.1016/j.advwatres.2015.11.008.

Salio, P., M. P. Hobouchian, Y. G. Skabar, and D. Vila, 2015: Evaluation of high-resolution satellite precipitation estimates over southern South America using a dense rain gauge network. *Atmos. Res.*, **163**, 146–161, doi:10.1016/j.atmosres.2014.11.017.

Sapiano, M. R. P., and P. A. Arkin, 2009: An intercomparison and validation of high-resolution satellite precipitation estimates with 3-hourly gauge data. *J. Hydrometeor.*, **10**, 149–166, doi:10.1175/2008JHM1052.1.

Seto, S., T. Iguchi, and R. Meneghini, 2011: Comparison of TRMM PR V6 and V7 focusing heavy rainfall. *2011 IEEE International Geoscience and Remote Sensing Symposium (IGARSS)*, IEEE, 2582–2585, doi:10.1109/Igarss.2011.6049769.

Shen, Y., A. Y. Xiong, Y. Wang, and P. P. Xie, 2010: Performance of high-resolution satellite precipitation products over China. *J. Geophys. Res.*, **115**, D02114, doi:10.1029/2009JD012097.

Shi, W. L., X. Z. Yu, W. G. Liao, Y. Wang, and B. Z. Jia, 2013: Spatial and temporal variability of daily precipitation concentration in the Lancang River basin, China. *J. Hydrol.*, **495**, 197–207, doi:10.1016/j.jhydrol.2013.05.002.

Shige, S., H. Sasaki, K. Okamoto, and T. Iguchi, 2006: Validation of rainfall estimates from the TRMM Precipitation Radar and Microwave Imager using a radiative transfer model: 1. Comparison of the version-5 and -6 products. *Geophys. Res. Lett.*, **33**, L13803, doi:10.1029/2006GL026350.

Sorooshian, S., K. L. Hsu, X. Gao, H. V. Gupta, B. Imam, and D. Braithwaite, 2000: Evaluation of PERSIANN system satellite-based estimates of tropical rainfall. *Bull. Amer. Meteor. Soc.*, **81**, 2035–2046, doi:10.1175/1520-0477(2000)081<2035:EOPSSE>2.3.CO;2.

Sun, R. C., H. L. Yuan, X. L. Liu, and X. M. Jiang, 2016: Evaluation of the latest satellite–gauge precipitation products and their hydrologic applications over the Huaihe River basin. *J. Hydrol.*, **536**, 302–319, doi:10.1016/j.jhydrol.2016.02.054.

Tan, M. L., A. Ibrahim, Z. Duan, A. P. Cracknell, and V. Chaplot, 2015: Evaluation of six high-resolution satellite and ground-based precipitation products over Malaysia. *Remote Sens.*, **7**, 1504–1528, doi:10.3390/rs70201504.

Tang, G. Q., Y. Z. Ma, D. Long, L. Z. Zhong, and Y. Hong, 2016a: Evaluation of GPM Day-1 IMERG and TMPA version-7 legacy products over mainland China at multiple spatio-temporal scales. *J. Hydrol.*, **533**, 152–167, doi:10.1016/j.jhydrol.2015.12.008.

——, Z. Y. Zeng, D. Long, X. L. Guo, B. Yong, W. H. Zhang, and Y. Hong, 2016b: Statistical and hydrological comparisons between TRMM and GPM level-3 products over a midlatitude basin: Is Day-1 IMERG a good successor for TMPA 3B42V7? *J. Hydrometeor.*, **17**, 121–137, doi:10.1175/JHM-D-15-0059.1.

Tapiador, F. J., and Coauthors, 2012: Global Precipitation Measurement: Methods, datasets and applications. *Atmos. Res.*, **104–105**, 70–97, doi:10.1016/j.atmosres.2011.10.021.

Tian, Y., Y. P. Xu, and X. J. Zhang, 2013: Assessment of climate change impacts on river high flows through comparative use of GR4J, HBV and Xinanjiang Models. *Water Resour. Manage.*, **27**, 2871–2888, doi:10.1007/s11269-013-0321-4.

Tong, K., F. G. Su, D. Q. Yang, and Z. C. Hao, 2014: Evaluation of satellite precipitation retrievals and their potential utilities in hydrologic modeling over the Tibetan Plateau. *J. Hydrol.*, **519A**, 423–437, doi:10.1016/j.jhydrol.2014.07.044.

Turk, F. J., G. V. Mostovoy, and V. G. Anantharaj, 2010: Soil moisture sensitivity to NRL-blend high-resolution precipitation products: Analysis of simulations with two land surface models. *IEEE J. Sel. Top. Appl. Earth Obs. Remote Sens.*, **3**, 32–48, doi:10.1109/JSTARS.2009.2034024.

Ushio, T., and Coauthors, 2009: A Kalman filter approach to the Global Satellite Mapping of Precipitation (GSMaP) from combined passive microwave and infrared radiometric data. *J. Meteor. Soc. Japan*, **87A**, 137–151, doi:10.2151/jmsj.87A.137.

Wanders, N., M. Pan, and E. F. Wood, 2015: Correction of real-time satellite precipitation with multi-sensor satellite observations of land surface variables. *Remote Sens. Environ.*, **160**, 206–221, doi:10.1016/j.rse.2015.01.016.

Wang, X. L., and A. Lin, 2015: An algorithm for integrating satellite precipitation estimates with in situ precipitation data on a pentad time scale. *J. Geophys. Res. Atmos.*, **120**, 3728–3744, doi:10.1002/2014JD022788.

Wolff, D. B., D. A. Marks, E. Amitai, D. S. Silberstein, B. L. Fisher, A. Tokay, J. Wang, and J. L. Pippitt, 2005: Ground validation for the Tropical Rainfall Measuring Mission (TRMM). *J. Atmos. Oceanic Technol.*, **22**, 365–380, doi:10.1175/JTECH1700.1.

Xu, S. G., C. Y. Wu, L. Wang, A. Gonsamo, Y. Shen, and Z. Niu, 2015: A new satellite-based monthly precipitation downscaling algorithm with non-stationary relationship between precipitation and land surface characteristics. *Remote Sens. Environ.*, **162**, 119–140, doi:10.1016/j.rse.2015.02.024.

Xue, X. W., Y. Hong, A. S. Limaye, J. J. Gourley, G. J. Huffman, S. I. Khan, C. Dorji, and S. Chen, 2013: Statistical and hydrological evaluation of TRMM-based Multi-Satellite Precipitation Analysis over the Wangchu basin of Bhutan: Are the latest satellite precipitation products 3B42V7 ready for use in ungauged basins? *J. Hydrol.*, **499**, 91–99, doi:10.1016/j.jhydrol.2013.06.042.

Yin, Z. Y., X. Q. Zhang, X. D. Liu, M. Colella, and X. L. Chen, 2008: An assessment of the biases of satellite rainfall estimates over the Tibetan Plateau and correction methods based on topographic analysis. *J. Hydrometeor.*, **9**, 301–326, doi:10.1175/2007JHM903.1.

Yong, B., L. L. Ren, Y. Hong, J. H. Wang, J. J. Gourley, S. H. Jiang, X. Chen, and W. Wang, 2010: Hydrologic evaluation of Multisatellite Precipitation Analysis standard precipitation products in basins beyond its inclined latitude band: A case study in Laohahe basin, China. *Water Resour. Res.*, **46**, W07542, doi:10.1029/2009WR008965.

——, D. Liu, J. J. Gourley, Y. D. Tian, G. J. Huffman, L. L. Ren, and Y. Hong, 2015: Global view of real-time TRMM Multisatellite Precipitation Analysis implications for its successor Global Precipitation Measurement mission. *Bull. Amer. Meteor. Soc.*, **96**, 283–296, doi:10.1175/BAMS-D-14-00017.1.

Zeng, H. W., L. J. Li, J. M. Hu, L. Q. Liang, J. Y. Li, B. Li, and K. Zhang, 2013: Accuracy validation of TRMM Multisatellite Precipitation Analysis daily precipitation products in the Lancang River basin of China. *Theor. Appl. Climatol.*, **112**, 389–401, doi:10.1007/s00704-012-0733-8.

Zhang, S. F., D. Hua, X. J. Meng, and Y. Y. Zhang, 2011: Climate change and its driving effect on the runoff in the ''Three-River Headwaters'' region. *J. Geogr. Sci.*, **21**, 963–978, doi:10.1007/s11442-011-0893-y.

Zhao, C. C., S. X. Yao, J. Wang, and J. B. Cui, 2013: Evaluation of satellite-based precipitation over Tianshan mountains. *Proc. 2013 Int. Conf. on Remote Sensing, Environment and Transportation Engineering (RSETE 2013)*, Nanjing, China, Jiangsu Computer Society, 957–960, doi:10.2991/rsete.2013.232.

Zhao, R.-J., 1992: The Xinanjiang model applied in China. *J. Hydrol.*, **135**, 371–381, doi:10.1016/0022-1694(92)90096-E.

Zhuo, L., D. W. Han, Q. Dai, T. Islam, and P. K. Srivastava, 2015: Appraisal of NLDAS-2 multi-model simulated soil moistures for hydrological modelling. *Water Resour. Manage.*, **29**, 3503–3517, doi:10.1007/s11269-015-1011-1.